Astronomy & Astrophysics manuscript no. paper
December 27, 2010

A spectroscopic survey of faint, high-galactic latitude red clump stars. II. The medium resolution sample

T. Saguner[1,2], U. Munari[1], M. Fiorucci[1] and A. Vallenari[1]

[1]INAF-OAPD-Osservatorio Astronomico di Padova, via dell'Osservatorio 8,I-36012 Asiago (VI), Italy
[2]University Of Padova, Department Of Astronomy, vicolo dell'Osservatorio 3, I-35122 Padova (PD), Italy

Received , 2010; accepted , 2010

ABSTRACT

Aims. The goal of our survey is to provide accurate and multi-epoch radial velocities, atmospheric parameters ($T_{\rm eff}$, $\log g$ and [M/H]), distances, and space velocities of faint red clump stars.
Methods. We recorded high signal-to-noise (S/N≥200) spectra of RC stars over the 4750-5950 Å range at a resolving power 5500. The target stars are distributed across the great circle of the celestial equator. Radial velocities were obtained via cross-correlation with IAU radial velocity standards. Atmospheric parameters were derived via χ^2 fit to a synthetic spectral library. A large number of RC stars from other surveys were re-observed to check the consistency of our results and the absence of offsets and trends.
Results. A total of 245 RC stars were observed (60 of them with a second epoch observation separated in time by about three months), and the results are presented in an output catalog. None of them is already present in other surveys of RC stars. In addition to astrometric and photometric support data from external sources, the catalog provides radial velocities (accuracy σ(RV)=1.3 km s^{-1}), atmospheric parameters ($\sigma(T_{\rm eff})$=88 K, $\sigma(\log g)$=0.38 dex and σ([M/H])=0.17 dex), spectro-photometric distances, (X,Y,Z) galacto-centric positions and (U,V,W) space velocities.

Key words. Galaxy: kinematics and dynamics - Galaxy: structure - Galaxy: solar neighborhood

1. Introduction

The Red Clump (RC) is composed by low mass stars in the stage of central helium burning, following He ignition in an electron-degenerate core (Girardi 1999). They display properties that make them a primary tool to investigate Galactic structure and kinematics: *(i)* their absolute magnitude shows minimal dispersion at optical and infrared wavelengths, *(ii)* they are intrinsically bright, and thus observable throughout most of the Galaxy, *(iii)* in magnitude-limited surveys they count for a fairly large fraction of observed targets, *(iv)* their spectral types, ranging mainly from G8III to K2III, make them ideal stars to measure accurate radial velocities and atmospheric chemical abundances. Examples of recent applications of RC stars to Galaxy investigations are, among countless more, the peculiarities of Galactic rotation (Rybka et al. 2008), the stellar bar in the inner Galaxy (Cabrera-Lavers et al. 2007), the Galactic Bulge (Nataf et al. 2010), the vertical distribution of disk stars in terms of kinematic and metallicity (Soubiran et al. 2003), the surface mass density in the Galactic plane (Siebert et al. 2003), the origin of the Thick disk (Ruchti et al. 2010), the surface mass density in the Galactic disk (Bienayme et al. 2006) and age-metallicity relation (AMR), age-velocity relation (AVR) (Soubiran et al. 2008), tidal streams in solar neighborhood (Famaey et al. 2005, Antoja et al. 2008), Galactic substructures (Correnti et al. 2010, Law et al. 2010). The large proportion of RC stars observed by the ongoing RAVE survey (Steinmetz et al. 2006, Zwitter et al. 2008) and the accurate distances derived for them (Zwitter et al. 2010) support a great potential of the RAVE data base in progressing towards a better understanding of how the Galaxy formed, structured and evolved (Freeman & Bland-Hawthorn 2002, Siebert et al. 2008, Veltz et al. 2008, Kiss et al. 2010).

This paper is an extension to fainter magnitudes of the spectroscopic survey of RC stars of Valentini & Munari (2010), hereafter named Paper I. Accurate radial velocities, atmospheric parameters ($T_{\rm eff}$, $\log g$, [M/H]), distances and space velocities have been obtained for 245 RC stars distributed along the great circle of celestial equator, 60 of them re-observed at a second epoch. These data are presented in a catalog together with photometric and astrometric support information from external sources.

The application to Galaxy investigations of the results obtained in this study and in Paper I will be the topic of a forthcoming paper.

2. Target selection criteria

To ensure the highest homogeneity within the present program, we adopted exactly the same target selection criteria as in Paper I, the only difference being an average magnitude of the target stars ∼1 mag fainter than in Paper I and consequently a ∼50% larger distance.

To summarize, the selection criteria are: *(i)* a star of spectral type between G8III and K2III as classified by the Michigan Project (Houk and Swift 1999), with *(ii)* a high accuracy in the spectral type (quality index ≤2), and *(iii)* a blank spectroscopic duplicity index. The stars must be *(iv)* uniformly distributed in right ascension within ±6° of the celestial equator (thus along a great circle on the sky), and at *(v)* Galactic latitude $|b|\geq 25°$ (to avoid the increasing reddening close to the plane of the Galaxy). In addition, the target stars must *(vi)* be valid entries

in both the Hipparcos[1] and Tycho-2 catalogs, *(vii)* have non-negative Hipparcos parallaxes, *(viii)* avoid any other Hipparcos or Tycho-2 star closer than 10 arcsec on the sky, *(ix)* be confined within the magnitude range $7.8 \leq V_{\rm Tycho2} \leq 9.5$ (for Paper I it was $6.8 \leq V_{\rm Tycho2} \leq 8.1$), *(x)* have an absolute magnitude (from Hipparcos parallax) incompatible with either luminosity classes V or I, *(xi)* have a blank photometric variability flag and a blank duplicity index in the Hipparcos catalog. Finally, the target stars must *(xii)* be present in the 2MASS survey, *(xiii)* be absent in the Nördstrom et al. (2004) Geneva-Copenhagen survey of dwarfs in the solar neighborhood, and *(xiv)* be absent in the radial velocity survey of giant stars by Famaey et al. (2005). Given the small overlap in magnitude with Paper I, we added a final selection criterion that *(xv)* no target from Paper I is re-observed here, to increase the total number of surveyed RC stars.

These selection criteria returned a total sample of 500 possible target stars.

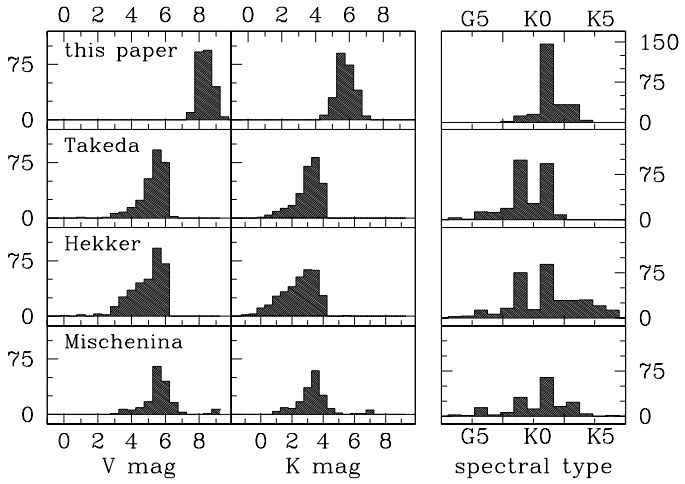

Fig. 1. Distribution in *V* and *K* band brightness, and in spectral type of our target stars and the RC surveyed by Takeda et al. (2008), Hekker & Melendez (2007), Mishenina et al. (2006).

3. Program stars

We have observed 245 target stars, 60 of them at two distinct epochs. Figure 1 compares their brightness distribution in *V*, *K*, and spectral type with those of other surveys of RC stars. The comparison with the program stars of Paper I is carried out in Fig. 2.

As for Paper I, we have re-observed a number of RC stars from other surveys with the same instrument set-up and reduction/analysis procedures. We re-observed 87 RC stars so selected: 47 from Hekker & Melendez (2007), 34 from Takeda et al. (2008) and 6 from Soubiran & Girard (2005). In addition, 15 IAU radial velocity standards (most of them RC stars) were observed too. This allowed us to check for zero-point offsets in the atmospheric parameters and radial velocity. These observations, supplemented by the results of repeated observations of our target stars, provided a consistent estimate of the errors associated to our measurements.

[1] All selection criteria involving Hipparcos information refer to the original catalog published by ESA in 1997, and not necessarily its revision by van Leeuwen (2007).

4. Observations and data reduction

The spectra were obtained from 2008 June to 2010 June with the 1.22m telescope + B&C spectrograph operated in Asiago by the Department of Astronomy of the University of Padova. The CCD camera was an ANDOR iDus 440A, equipped with an EEV 42-10BU back-illuminated chip, 2048×512 pixels of 13.5 μm size. A 1200 ln/mm grating provided a scale of 0.61 Å/pix and the recorded wavelength range extended from 4750 to 5950 Å. A slit width of 2 arcsec provided a resolving power close to 5500, or a resolution of about 1.0 Å. The exposure time was kept fixed to 600 sec for all target stars, which provided a S/N≥200 on the final extracted spectra at the faint end of the magnitude distribution of our program stars. For the brighter template RC stars selected from literature and the IAU radial velocity stars, shorter exposure times were adopted to avoid approaching CCD saturation levels. All target stars were observed within 1 hour of their culmination time.

The 4750 to 5950 Å wavelength range includes the Hβ, Mg*b* triplet and NaI $D_{1,2}$ doublet regions. Preliminary to initiating the observations of the target RC stars, we experimented with bluer and redder wavelength ranges by extensively observing the same selected template RC stars. Bluer ranges suffered from a marked reduction in the S/N of extracted spectra (lower target brightness and overall instrumental throughput) and a more difficult continuum normalization owing to increased density of absorption lines. The lower density of absorption lines of redder wavelenth ranges offered the advantage of an easier continuum normalization, but at the expense of a lower diagnostic content for measurement of atmospheric parameters and radial velocities. If the two effects roughly balanced a marked disadvantage of redder wavelenth ranges is the presence of telluric absorption lines and bands which significantly alter the response of χ^2 fits to synthetic spectra. Eventually, the 4750 to 5950 Å wavelength range was selected as the best-performing interval.

The data reduction was carried out in *IRAF*, following in detail the standard procedures described in the manual by Zwitter & Munari (2000), which involved correction for bias (from overscan regions), dark and flat-field frames (from exposure on the dome), sky-background subtraction (our long-slit mode extends for 1 arcmin on the sky), scattered light removal, wavelength calibration (from Fe-Ar comparison lamp frames exposed immediately before and after the science exposure, with the telescope tracking the star) and heliocentric correction.

At least three IAU radial velocity standards were observed at very high S/N during each night to allow the derivation of the radial velocity of program stars via cross-correlation techniques.

4.1. Continuum Normalization

The determination of radial velocities via cross-correlation, and in particular the derivation of atmospheric parameters via χ^2 fitting, critically depend on the accuracy of continuum normalization. To ensure the highest quality, control, and homogeneity, the continuum normalization of all spectra was carried out manually as a three-step procedure.

First of all, a lot of care was put in training the operator's human response. To this aim, we used the synthetic spectral library of Munari et al. (2005). It covers the whole parameter space of the HR diagram and comes in many different resolving powers, one of which exactly matches that of our spectra. The synthetic library provides the same spectra computed both as absolute fluxes and as continuum normalized. About 100 synthetic spectra similar to those of RC stars and of the absolute-flux type

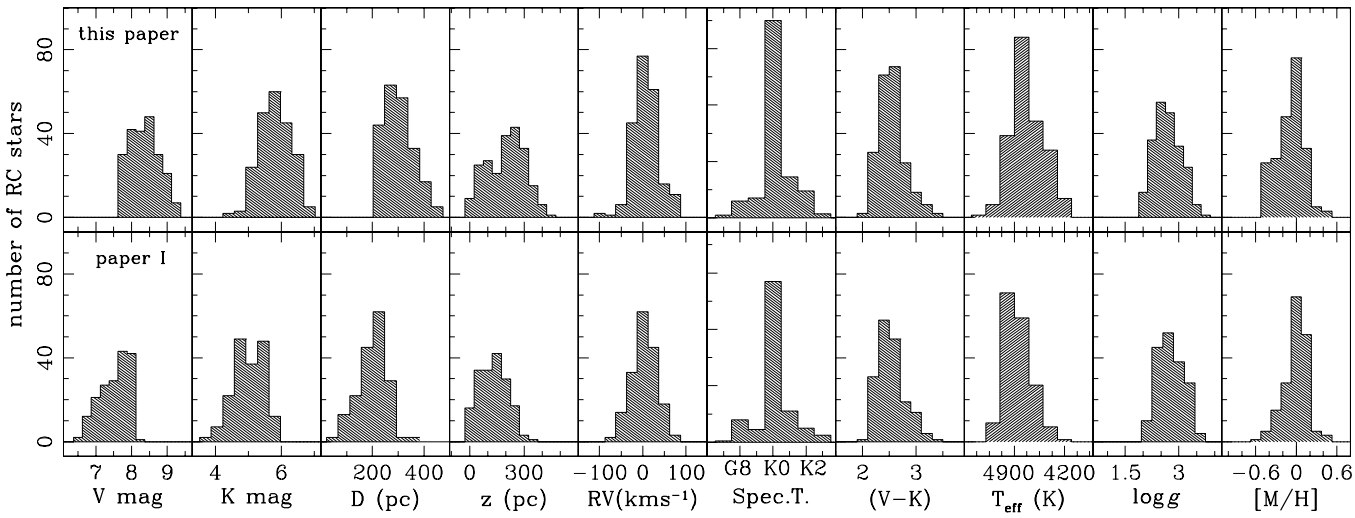

Fig. 2. Comparison of the distribution in various parameters of the stars investigated here and in Paper I.

Table 1. Comparison for the program 15 IAU RV standards between the tabulated heliocentric radial velocity and that measured in our spectra.

Star	Spc.T.	Literature		Cross-Correlation	
		$RV_\odot$	err.	$RV_\odot$	σ_{RV}
HD 4388	K3 III	−28.3	0.6	−27.4	2.1
HD 62509	K0 III	03.3	0.1	02.3	2.7
HD 132737	K0 III	−24.1	0.3	−25.0	1.6
HD 136202	F8 III	53.5	0.2	48.6	1.9
HD 144579	G8 IV	−60.0	0.3	−62.5	0.8
HD 145001	G5 III	−09.5	0.2	−10.5	1.2
HD 154417	F8 IV	−17.4	0.3	−15.3	1.5
HD 161096	K2 III	−12.0	0.1	−13.6	0.9
HD 182572	G7 IV	−100.5	0.5	−102.1	1.1
HD 187691	F8 V	00.1	0.3	02.6	0.8
HD 194071	G8 III	−09.8	0.1	−06.9	0.5
HD 212943	K0 III	54.3	0.3	55.9	1.9
HD 213014	G9 III	−39.7	0.0	−37.4	1.7
HD 213947	K2	16.7	0.3	17.5	1.3
BD+28.3402	F7 V	−36.6	0.5	−36.5	0.4

where selected from the synthetic library. They were multiplied by randomly selected, arbitrary instrumental response functions, and noise was added to simulate the S/N≥200 that characterizes our observed spectra. The resulting spectra were then manually normalized with the IRAF task CONTINUUM. To close the loop, the result of the normalization was compared with the synthetic spectrum originally computed as continuum normalized. The comparison easily revealed where improvements in the human decision chain were necessary, and by a tedious - but also effective - trial-and-error procedure, a relevant experience and confidence in the results was built. On average, the best results were obtained with a Legendre fitting polynomial of 5^{th} order, a high-rejection threshold of 0.0 and a low-rejection threshold of 1.35×sigma.

The second step was to apply this human experience to the observed spectra, normalizing them manually and individually with the same IRAF task, and whenever appropriate adopting the same fitting polynomials and associated parameters. In some cases, a different degree for the polynomial, or masking of some portion of the spectrum, or changes of other parameters were necessary for an optimal result, depending on the specific characteristic of individual observed spectra.

The third and final step was to automatically renormalize with the same IRAF task CONTINUUM and associated parameters the whole Munari et al. (2005) library of synthetic spectra, so they would probably speak the same language as the observed ones. Before running the χ^2 a final refinement was applied by imposing that the geometric mean of each synthetic spectrum matched that of the observed one (this forced the mean level of the continuum in the observed and synthetic spectra to coincide).

5. Data quality control

The wavelength range covered by our spectra includes four appreciably intense night-sky and city-lights lines, namely [OI] 5577.333, and HgI 5460.734, 5769.579, 5790.643 Å. We measured them on all recorded spectra to check the wavelength calibration from their radial velocity and the spectrograph focusing from their sharpness. During data analysis we noticed that the spectra characterized by a FWHM≤2.0 Å for the night-sky lines, invariably returned the radial velocity of the night sky lines as |RV|<1.8 km s^{-1}, independently of the FWHM. The spectra with FWHM>2.0 Å, showed instead a larger dispersion of the radial velocity of the night sky lines, which increased with increasing FWHM.

The same dividing threshold affected the accuracy of radial velocities and atmospheric parameters obtained for the target stars. Comparing the results of repeated observations of the same targets, spectra characterized by a FWHM≤2.0 Å for the night-sky lines showed a well behaving, sharp, and Gaussian distribution of the differences (see Figures 3 and 5, and text below), which could not be further improved by a stricter limit imposed on the FWHM of the night-sky lines. Conversely, spectra with FWHM>2.0 Å showed larger dispersion in the differences between 1^{st} and 2^{nd} observations, clearly tracing a different and looser statistical population.

Because we are interested only in the best products our instrumentation could deliver, we ignored all observations characterized by a FWHM>2.0 Å for the night-sky emission lines, and they will not be further considered in this paper. This meant re-

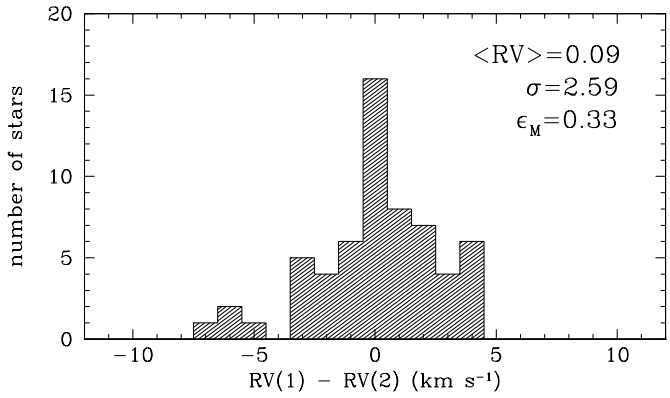

Fig. 3. Distribution of the differences in radial velocity between repeated observations.

ducing by 43 objects the number of targets inserted in the paper's output catalog, which in its final version includes 245 RC target stars.

6. Radial velocities

The radial velocity for our target stars was obtained via cross-correlation against a set of RC stars that were also IAU radial velocity standard stars. At least three such standards were observed each night together with the target stars. The radial velocity of the latter was obtained as the mean of the cross-correlation results against all standards observed that night.

The cross-correlation was performed in IRAF with the task FXCOR. About 20 Å were masked at both ends of the spectra, because there the accuracy of wavelength calibration and continuum normalization degrades for obvious reasons.

6.1. Tests on RV standards

To test the accuracy of our radial velocities, we selected the sample of 15 bright IAU radial velocity standards listed in Table 1. We observed them during four different nights. For each night and for each standard the radial velocity was derived by cross-correlation against all other standards observed that same night. The last two columns of Table 1 given the mean value and the dispersion of the individual values.

The median dispersion of these measurement is 1.36 km s^{-1}. Considering that the mean uncertainty of the tabulated radial velocities is 0.27 km s^{-1}, we may conclude that the accuracy of our radial velocities is 1.3 km s^{-1}.

The zero point of our radial velocities is not biased. In fact, the mean difference between observed and published radial velocity for the 15 standards in Table 1 is only +0.04 km s^{-1}, with an error of the mean of 0.55 and a dispersion of 2.1 km s^{-1}.

6.2. Tests with multi-epoch observation

As noted in Sect. 3, 60 of the 245 target stars were observed at a second epoch, typically at least three months apart. The comparison of first and second epoch observations offers another test of the accuracy and consistency of the radial velocity provided in the catalog associated to this paper.

The comparison is presented in Figure 3, which indicates a negligible value for the mean difference between the velocities at the two epochs and a standard deviation of the differences amounting to 2.6 km s^{-1}.

Table 2. Comparison between the atmospheric parameters obtained with the χ^2 method and those derived by Hekker and Melendez (2007)

HD	Spc.T.	Hekker & Melendez			χ^2		
		$T_{\rm eff}$ (K)	log$g$ (dex)	[M/H] (dex)	$T_{\rm eff}$ (K)	log$g$ (dex)	[M/H] (dex)
3807	K0 III	4625	2.30	−0.44	4526	1.80	−0.46
4627	G8 III	4599	2.05	−0.25	4664	2.42	−0.04
6186	K0 III	4829	2.30	−0.24	4845	2.55	−0.50
7087	K0 III	4850	2.55	−0.15	4915	2.74	−0.12
7318	K0 III	4815	2.55	−0.11	4832	2.50	−0.08
10380	K3 III	4300	2.20	−0.27	4410	1.99	0.00
10761	K0 III	4952	2.43	0.00	5020	2.84	−0.24
12929	K2 III	4600	2.70	−0.13	4480	2.28	−0.04
13468	G9 III	4893	2.54	−0.12	4919	2.64	−0.42
15176	K1 III	4650	2.85	−0.07	4531	2.45	−0.08
18449	K2 III	4500	2.65	−0.07	4314	2.30	0.00
19656	K1 III	4600	2.30	−0.18	4726	2.46	0.00
21755	G8 III	5012	2.45	−0.03	5064	2.95	−0.38
26162	K2 III	4800	2.90	0.06	4728	2.76	0.00
27382	K1 III	4550	2.50	−0.32	4371	1.67	−0.46
27697	G8 III	4984	2.64	0.09	4955	3.06	0.00
28100	G8 III	5011	2.54	−0.24	5039	3.17	−0.33
28305	K0 III	4883	2.57	0.05	4976	3.06	0.00
34559	G8 III	4998	2.74	0.03	5084	3.20	−0.12
38527	G8 III	5046	2.77	−0.07	5122	3.29	−0.29
42398	K0 III	4650	2.40	−0.15	4646	2.51	−0.17
48433	K1 III	4550	2.20	−0.20	4528	2.15	0.00
52556	K1 III	4700	2.65	−0.08	4627	2.55	0.00
54079	K0 III	4450	2.10	−0.42	4415	1.85	−0.38
54719	K2 III	4500	2.55	0.14	4512	2.35	0.29
55751	K0 III	4550	2.10	−0.11	4619	2.28	0.00
59686	K2 III	4650	2.75	0.15	4706	2.51	0.00
65695	K2 III	4470	2.45	−0.15	4436	2.14	0.00
69994	K1 III	4650	2.60	−0.07	4518	2.38	−0.08
73471	K2 III	4550	2.40	0.05	4603	2.66	0.29
184406	K3 III	4520	2.41	0.04	4356	2.36	0.06
190327	K0 III	4850	2.70	−0.15	4832	2.83	0.18
192944	G8 III	5000	2.70	−0.10	5040	2.84	−0.08
194317	K3 III	4435	2.70	0.04	4338	2.73	0.12
197139	K2 III	4485	2.40	−0.08	4439	1.87	−0.04
197912	K0 III	4940	3.17	−0.03	4844	2.77	−0.06
197989	K0 III	4785	2.27	−0.11	4791	2.25	−0.04
199253	K0 III	4625	2.35	−0.19	4520	2.49	0.00
209761	K2 III	4420	2.35	−0.08	4371	1.98	0.00
210762	K0 III	4185	1.65	0.00	4181	1.98	0.42
211388	K3 III	4260	2.15	0.01	4173	1.48	0.46
213119	K5 III	3910	1.59	−0.48	3955	1.34	−0.37
214995	K0 III	4680	2.70	−0.04	4540	2.25	0.13
219615	G7 III	4830	2.57	−0.54	4958	2.26	−0.50
220954	K1 III	4775	2.95	0.02	4779	2.51	0.00
223252	G8 III	5031	2.72	−0.08	5041	2.88	−0.12
224533	G9 III	5030	2.72	−0.02	5084	2.87	−0.04

It is interesting to note that none of the 60 stars in Figure 3 shows a radial velocity difference between first and second epoch exceeding 3σ, indicating that all observed differences could be entirely ascribed to only observational uncertainties, without necessarily invoking binarity or pulsation.

7. Atmospheric parameters

We derived the atmospheric parameters ($T_{\rm eff}$, $\log g$, [M/H]) of program stars via χ^2 fitting to the synthetic spectral library of Munari et al. (2005), the same library as used in the analysis of RAVE spectra, which is based on the atmospheric models of Castelli & Kurucz (2003). We used the library in its solar scaled ($[\alpha/Fe] = 0$) and 2 km s^{-1} micro-turbulence version, computed at a resolving power 5500, the same as our observed spectra.

7.1. Selecting the wavelength range for χ^2

We carried out extensive preliminary tests to investigate what should be the optimal extension and positioning of the wavelength interval within the recorded wavelength range over which to carry out the χ^2 fitting.

The necessity of such a preliminary assessment was dictated by some considerations. On one side, the wider the wavelength range subject to χ^2, the larger the amount of information brought in. On the other hand, the wider the wavelength range, the less trustworthy is the continuum normalization. In addition, while the χ^2 fitting is mainly driven by the countless amount of weak, optically thin lines forming over a large extension of the stellar atmosphere, the classical line-by-line analysis (usually based on ionization and excitation balance of Fe lines) works on a selected and limited sample of lines that could probe a less extended depth of the stellar atmosphere. Furthermore, while χ^2 fitting is a far more efficient method with large volumes of data and/or with medium (or low) resolution spectra that are packed with blended lines, it is also far more sensitive than the line-by-line method to the limited completeness of the line lists used to compute the synthetic spectra (see for example the huge number of *new* FeII lines introduced by Castelli and Kurucz 2010).

For these and other subtler reasons we extensively explored what could be gained by considering only a sub-interval of the whole wavelength range covered by our spectra.

To this aim, we used the spectra of the 87 RC stars that we selected from the extensive surveys of RC stars by Hekker & Melendez (2007), Takeda et al. (2008) and Soubiran & Girard (2005), and which we re-observed with our instrument with the same S/N of the spectra collected for the target stars (see next section for details). The atmospheric analysis in these papers was carried out on high-resolution spectra with the line-by-line method. We considered wavelength intervals progressively shorter (in steps of 100 Å), and let them reposition freely within the recorded wavelength range of our spectra. For each spectrum and for each length and position of the wavelength interval we compared the result of the χ^2 fitting with that of the line-by-line method.

The results of the comparison showed that the accuracy of the χ^2 fitting does not improve by considering wavelength intervals wider than 300 Å. Next, we explored what would be the best positioning of a $\Delta\lambda$=300 Å interval that would minimize the difference between the results of χ^2 fitting and literature data based on the line-by-line method. We found that the interval 4761−5061 Å delivered the best results (in the sense of null off-set and lower dispersion) for [M/H], 5614−5918 Å for $\log g$, and 5012−5312 Å for $T_{\rm eff}$. These intervals were consequently adopted for the analysis of target stars.

Table 3. Comparison between the atmospheric parameters obtained with the χ^2 method and those derived by Takeda et al. (2008)

HD	Spc.T.	Takeda			χ^2		
		$T_{\rm eff}$ (K)	log$g$ (dex)	[M/H] (dex)	$T_{\rm eff}$ (K)	log$g$ (dex)	[M/H] (dex)
448	G9 III	4780	2.51	0.03	4731	2.63	0.04
587	K1 III	4893	3.08	−0.09	4791	3.25	−0.34
4627	G8 III	4599	2.05	−0.20	4664	2.42	−0.04
6186	K0 III	4829	2.30	−0.31	4845	2.55	−0.50
7087	K0 III	4850	2.55	−0.04	4915	2.74	−0.12
10348	K0 III	4931	2.55	0.01	4895	3.06	0.00
10761	K0 III	4952	2.43	−0.05	5020	2.84	−0.24
10975	K0 III	4866	2.47	−0.17	4874	2.68	−0.25
11037	G9 III	4862	2.45	−0.14	4957	2.51	−0.37
13468	G9 III	4893	2.54	−0.16	4919	2.64	−0.42
19525	G9 III	4801	2.59	−0.11	4813	2.69	−0.08
21755	G8 III	5012	2.45	−0.13	5064	2.95	−0.38
23526	G9 III	4837	2.50	−0.15	4852	2.63	−0.42
27371	G8 III	4923	2.57	0.10	4985	3.21	0.00
27697	G8 III	4984	2.64	0.12	4955	3.06	0.00
28100	G8 III	5011	2.54	−0.08	5039	3.17	−0.33
28305	K0 III	4883	2.57	0.13	4976	3.05	0.00
34559	G8 III	4998	2.74	0.00	5084	3.20	−0.12
35410	K0 III	4809	2.58	−0.33	4794	2.94	−0.50
38527	G8 III	5046	2.77	−0.11	5122	3.29	−0.29
39007	G8 III	4994	2.69	0.08	5148	3.30	0.00
39019	G9 III	4964	2.91	0.19	5017	3.25	0.00
45415	G9 III	4753	2.39	−0.12	4852	2.73	−0.25
51814	G8 III	4846	2.23	−0.02	4753	2.79	−0.04
192787	K0 III	5025	2.86	−0.07	4958	2.76	−0.12
192944	G8 III	4981	2.48	−0.06	5040	2.84	−0.08
209396	K0 III	4999	2.81	0.04	5041	3.17	−0.04
210434	K0 III	4949	2.93	0.12	4919	3.13	0.08
210702	K1 III	4967	3.19	0.01	4974	3.21	−0.12
217264	K1 III	4946	2.80	0.12	4978	3.27	0.00
219615	G7 III	4802	2.25	−0.62	4958	2.26	−0.50
223252	G8 III	5031	2.72	−0.03	5041	2.88	−0.12
224533	G9 III	5030	2.72	−0.01	5084	2.87	−0.04

Table 4. Comparison between the atmospheric parameters obtained with the χ^2 method and those derived by Soubiran & Girard (2005)

HD	Spc.T.	Soubiran & Girardi			χ^2		
		$T_{\rm eff}$ (K)	log$g$ (dex)	[M/H] (dex)	$T_{\rm eff}$ (K)	log$g$ (dex)	[M/H] (dex)
188512	G8 IV	5106	3.54	−0.15	5073	3.42	−0.46
190404	K1 V	4963	3.90	−0.82	4539	3.44	−0.66
191026	K0 IV	5050	3.49	−0.10	4979	3.40	−0.25
197964	K1 IV	4813	3.03	0.17	4773	3.13	0.46
212943	K0 III	4586	2.81	−0.34	4521	2.50	−0.29
219615	G7 III	4830	2.57	−0.42	4958	2.26	−0.50

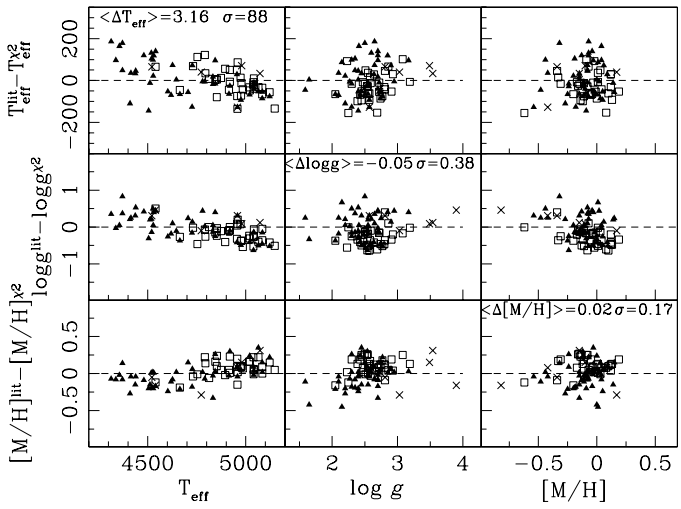

Fig. 4. Differences with literature for the atmospheric parameters derived from χ^2 fitting for 87 red clump stars. Empty squares are stars from Takeda et al. (2008), filled triangles Hekker & Melendez (1997) and the crosses from Soubiran & Girard (2005).

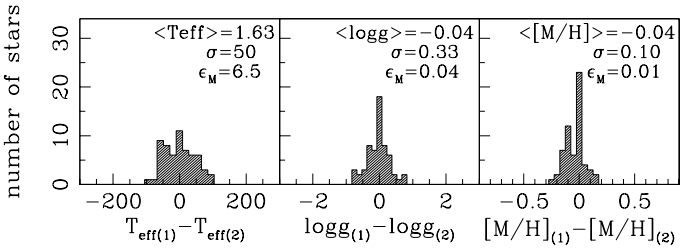

Fig. 5. The differences in effective temperature, gravity and metallicity of repeated observations of 60 target stars.

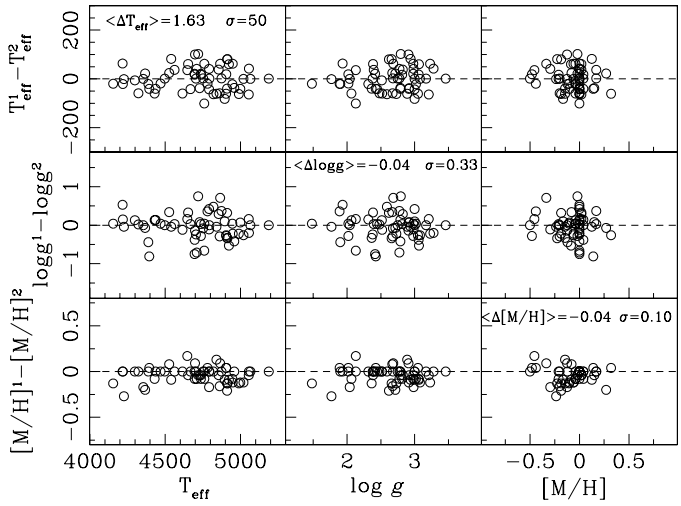

Fig. 6. Distribution of the differences in atmospheric parameters for repeated observations of 60 RC stars .

7.2. Comparison with literature data on red clump stars

To test the accuracy of the results of our χ^2 fitting, a comparison was carried out against the results of existing surveys of RC stars.

Hekker & Melendez (2007), Takeda et al. (2008) and Soubiran & Girard (2005) provided detailed chemical abundance analyses of RC stars. Based solely on observability at the telescope, we selected 47 RC stars from Hekker & Melendez and 34 RC stars from Takeda et al., and observed them interspersed with the targets stars. The exposure time was adjusted so that the S/N of the spectra for these template stars would match the median value of the S/N obtained from the target stars (to avoid introducing biases, expecially during the continuum normalization process). This sample of template stars was augmented by an additional six stars in the same spectral type range of RC stars, but of various luminosity classes, selected from Soubiran & Girard.

The result of the comparison is given in Tables 2, 3, and 4, and presented in graphical form in Figure 4. For the whole sam-

Table 5. Content and description of the catalog

Character	Code	Units	Symbol	Description
1-8	I8	...	HD	HD number
9-15	I5	...	HIP	HIP number
16-21	I6	...	TYC1	TYCHO-2 1st identi???er
25-30	I5	...	TYC2	TYCHO-2 2nd identi???er
33	I1	...	TYC3	TYCHO-2 3rd identi???er
37-45	A11	...	spTyp	Spectral type from Michigan catalog
49-61	F12.8	...	RA	Right ascension (J2000)
65-77	F12.8	...	DE	Declination (J2000)
82-90	F8.4	deg	GLat	Galactic latitude
94-102	F8.4	deg	DLon	Galactic longitude
106-112	F6.4	mag	Hp	Hipparcos Hp magnitude
114-120	F6.4	mag	eHp	error on Hp
122-126	F4.2	mag	V-I	(V???I)C from Hipparcos catalog
130-134	F4.2	mag	eV-I	error on (V???I)C
137-141	F7.2	mas	parHip	Hipparcos (ESA 1997) parallax
143-147	F6.2	mas	eparHip	error on Hipparcos (ESA 1997) parallax
154-158	F7.2	mas	parVL	Hipparcos (van Leeuwen 2007) parallax
163-167	F6.2	mas	eparVL	error Hipparcos (van Leeuwen 2007) parallax
169-175	F6.3	mag	BT	Tycho BT magnitude
178-183	F5.3	mag	eBT	error on Tycho BT magnitude
186-191	F6.3	mag	VT	Tycho VT magnitude
194-199	F5.3	mag	eVT	error on Tycho VT magnitude
201-207	F6.1	mas/yr	pmRA	Tycho-2 RA proper motion
211-213	F4.1	mas/yr	epmRA	error on Tycho-2 RA proper motion
215-221	F6.1	mas/yr	pmDEC	Tycho-2 DEC proper motion
223-226	F4.1	mas/yr	epmDEC	error on Tycho-2 DEC proper motion
230-235	F6.3	mag	J2MASS	2MASS J magnitude
242-247	F5.3	mag	eJ2MASS	error on 2MASS J magnitude
250-255	F6.3	mag	K2MASS	2MASS H magnitude
258-263	F5.3	mag	eK2MASS	error on 2MASS H magnitude
266-271	F6.3	mag	K2MASS	2MASS K magnitude
274-279	F5.3	mag	eK2MASS	error on 2MASS K magnitude
281-284	A3	...	2MASSQF	2MASS quality index
286-291	F6.3	mag	IDENIS	DENIS I magnitude
298-302	F4.2	mag	eIDENIS	error on IDENIS
305-308	I3	...	DENISQF	DENIS quality index
311-327	F16.8	...	HJD	Heliocentric Julian date of Observation
330-334	F4.2	...	FWHM	FWHM of the night sky lines
336-341	F5.1	...	S/N	S/N ratio of the spectra
343-349	F6.1	(km s^{-1})	RV	Heliocentric radial velocity
354-357	F3.1	(km s^{-1})	eRV	Error on heliocentric radial velocity
362-366	I5	K	Teff	Effective temperature
371-374	I2	K	eTeff	Error on effective temperature
379-383	F4.2	dex	logg	Surface gravity
388-392	F5.2	dex	elogg	Error on surface gravity
398-403	F5.2	dex	[M/H]	Metallicity
408-412	F4.2	dex	e[M/H]	Error on metallicity
419-424	F6.1	pc	d	Spectrophotometric distance
429-433	F5.1	pc	ed	Error on spectro-photometric distance
437-445	F8.6	mag	Av	Extinction in *V*-band
448-457	F9.4	pc	X	Galactic X Coordinate
459-468	F9.4	pc	Y	Galactic Y coordinate
470-479	F9.4	pc	Z	Galactic Z coordinate
482-491	F8.4	(km s^{-1})	U	U velocity
492-502	F8.4	(km s^{-1})	V	V velocity
505-514	F8.4	(km s^{-1})	W	W velocity

ple of 87 template stars, it is

$$< (T_{\rm our} - T_{\rm lit}) > \; = \; +3 \; {\rm K} \quad (\sigma = 88 \; {\rm K}) \qquad (1)$$

$$< (\log g_{\rm our} - \log g_{\rm lit}) > \; = \; -0.05 \quad (\sigma = 0.38) \qquad (2)$$

$$< [{\rm M/H}]_{\rm our} - [{\rm M/H}]_{\rm lit} > \; = \; +0.02 \quad (\sigma = 0.17), \qquad (3)$$

thus negligible zero-point offsets, and limited dispersions. The latter could be even better if it were not inflated by the systematic differences between the individual sources in literature. Indeed considering the differences with individual sources, for the 47 RC stars in common with Hekker & Melendez (2007) we have $<(T_{\rm our}-T_{\rm HM})>= -11$ K (σ=83 K), $<(\log g_{\rm our}-\log g_{\rm HM})> = -0.06$ dex (σ=0.38 dex), $<([{\rm M/H}]_{\rm our}-[{\rm M/H}]_{\rm HM})> = 0.04$ (σ= 0.18), while the comparison with the 34 RC stars from Takeda et al. (2008) provides $<(T_{\rm our}-T_{\rm Tak})> =28$ K (σ=61 K), $<(\log g_{\rm our}-\log g_{\rm Tak})>=0.28$ (σ=0.23), $<([{\rm M/H}]_{\rm our}-[{\rm M/H}]_{\rm Tak})>=-0.10$ (σ= 0.11). For the 147 stars in common among them, $T_{\rm eff}$ and $\log g$ from Takeda et al. (2008) are on average ∼50 K cooler and ∼0.25 dex lower, respectively, than those of Hekker & Melendez (2007). These differences are close to those we found in this paper, with Takeda et al. (2008) being 39 K cooler and 0.34 dex lighter in gravity than Hekker & Melendez (2007).

7.3. Repeated observations

As discussed in Sect. 3, we re-observed 60 target RC stars at a second epoch, separated in time from the first observations by three months on average. Figure 5 presents the distribution of the differences in $T_{\rm eff}$, $\log g$ and [M/H] between these two re-observations. The distributions in all three parameters are sharp and well behaving. They are characterized by $\sigma(T_{\rm eff})$=50 K, $\sigma(\log g)$=0.33 dex and σ([M/H])=0.10 dex. The behavior of the differences versus $T_{\rm eff}$, $\log_g$ are illustrated in Figure 6. As for the observations of the 87 template stars, the differences do not show a trend with the atmospheric parameters.

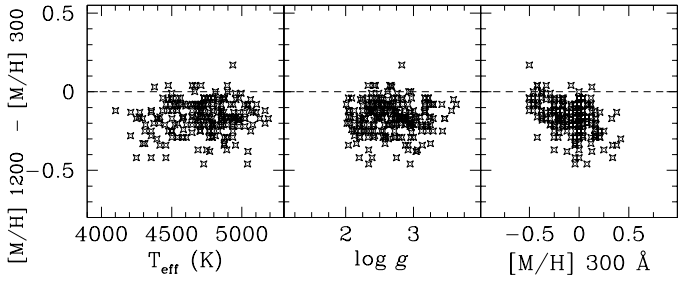

Fig. 7. Testing the difference in metallicity induced by widening the wavelength range for χ^2 fit from the adopted 300 Å to the 1200 Å covered by untrimmed spectra.

7.4. The absence of an off-set in metallicity

In Paper I we found and corrected for a systematic off-set in metallicity by −0.21 dex. The data in the present paper are not affected by a systematic off-set, and therefore no correction was added to the χ^2 results when compiling the output catalog.

Both Paper I and this study used the same χ^2 algorithm and the same reference library of synthetic spectra, and thus some investigation was in order to understand why the two papers show different results in terms of the presence/absence of an off-set in metallicity. To this aim, we carried out an additional χ^2 fit to the spectra discussed in this paper, this time taking the whole 1200 Å observed wavelength range, instead of the $\Delta\lambda$=300 Å adopted for the compilation of the annexed catalog. The untrimmed 1200 Å range of our spectra is the same range of wavelengths covered by the Echelle orders used in Paper I. As remarked earlier, the spectra extending over the whole 1200 Å range show locally deep and broad inflections owing to the presence of molecules, in particular MgH and CN. Guessing the true level of the continuum during the normalization process is far more uncertain in these conditions than for the shorter, 300 Å wide intervals used in this paper to derive the atmospheric parameters.

Figure 7 presents the difference in metallicity (Δ[M/H]) of χ^2 fits carried out over the whole 1200 Å range and over the 300 Å interval selected to measure the stellar metallicity. As expected, there is no systematics depending on $T_{\rm eff}$ and $\log g$ of the star, while a clear one is present on metallicity, in the sense that the higher the metallicity, the larger is the difference. The mean value of the difference is −0.16 dex, similar in sign and amount to the offset found for the Echelle spectra of Paper I. Extrapolating the linear trend visible in Fig. 7, Δ[M/H] is expected to null out at about [M/H]=−0.8. The interpretation seems straightforward. The continuum normalization process carried out unconstrained over the whole 1200 Å range tends to slightly fill in the molecular bands, causing the χ^2 to react by returning a reduced metallicity. A lower metallicity weakens the intensity of the molecular bands, and consequently the normalization process has less chance to fill in these bands. At [M/H]=−0.8 the molecular bands are too weak to drive the normalization of the stellar continua off-road prior to feeding the spectra to the χ^2 fitting routine.

8. The catalog

The results of our observations are presented in the output catalog (available electronically via CDS). We tried to make it as similar as possible to that accompanying Paper I. The major difference is that we do not provide a projected rotation velocity, given the lower resolution of our spectra. The catalog is divided into two parts, with observations for all 245 target stars going into the first part, and the second reporting the results of the re-observations for 60 targets. The content of the catalog is given in Table 5.

In addition to photometric and astrometric data from the literature, the catalog provides the distance, the U,V,W space velocities and the X,Y,Z galacto-centric coordinates of the target stars. These values were computed exactly as in Paper I, where full details are provided. In essence, we derived uniform spectrophotometric distances for all our program stars, adopting the intrinsic absolute magnitudes in the Johnson V band calibrated by Keenan & Barnbaum (2000). These absolute magnitudes are given separately for the various spectral types (G8III to K2III) covered by our program stars, and are calibrated on RC stars with the most precise Hipparcos parallaxes. To derive the distances, we transformed the Tycho-2 $V_{\rm T}$ into the corresponding Johnson V band following Bessell (2000) relations, and adopted the (always very low) reddening derived from the all-sky 3D mapping by Arenou et al. (1992) and Drimmel et al. (2003). The U, V, W velocities were derived from position (α, δ), proper motion (μ_α, μ_δ), radial velocity, and distance following the formalism of Johnson and Soderblom (1987). We adopted a left-handed system with U becoming positive outward from the Galactic center. We adopted for the Sun velocity components with respect

to the LSR the values found by Dehnen & Binney (1998, in km sec^{-1}): $U_{\odot}$=−10.0, $V_{\odot}$=5.23, $W_{\odot}$=7.17.

Acknowledgements. We would like to thank A. Siviero, M. Valentini, K. Freeman, and R. Barbon for their help; and P. Rafanelli, S. Ciroi, S. Di Mille and M. Fiaschi for supporting and encouraging observations with the Asiago telescopes. TS has been supported by ELSA (European Leadership in Space Astrometry) Marie Curie grant under FP6 contract MRTN-CT-2006-033481.

References

Antoja, T. et al., 2008, A&A 490, 135
Arenou, F., Grenon, M., & Gomez, A. 1992, A&A, 258, 104
Bessell, M. S. 2000, PASP, 112, 961
Cabrera-Lavers, A. et al., 2007, A&A 465, 825
Correnti, M. et al., 2010, ApJ 721, 329
Bienayme, O., Soubiran, C., Mishenina, T. V.,Kovtyukh, V. V., Siebert, A., 2006, A&A 446, 933
Castelli, F. , & Kurucz, R. L. 2003, in Modelling Of Stellar Atmospheres, N. Piskunov, W.W. Weiss, and D.F. Gray. eds., IAU Symp 210, Astronomical Society of the Pacific, S. Francisco, p. 20A
Castelli, F., & Kurucz, R. L. 2010, A&A, 520, A57
Dehnen, W., & Binney, J. J. 1998, MNRAS, 298 387
Drimmel, R., Cabrera-Lavers, A., & López-Corredoira, M. 2003, A&A, 409, 205
Famaey, B., Jorissen, A., Luri, X., Mayor,M., Udry, S., Dejonghe, H., Turon, C., 2005, ESA SP-576, 129
Freeman, K., & Bland-Hawthorn, J. 2002, ARA&A, 40, 487
Girardi, L. 1999, MNRAS, 308 818
Hekker, S.& Melendez, J., 2007, A&A 475, 1003
Houk, N., & Swift, C. 1999, Michigan catalogue of two-dimensional spectral types for the HD Stars, Department of Astronomy, University of Michigan
Keenan, P.C. & Barnbaum, C., 1999, ApJ 518, 859
Kiss, L. L., et al. 2010, MNRAS, in press (tmp1636)
Johnson, D. R. H., & Soderblom, D. R. 1987, AJ, 93, 864
Law, D.R., Majewski, S. R., Johnston, K. V., 2010, AAS, 21532103
Munari, U., Sordo, R., Castelli, F.,& Zwitter, T., 2005, A&A 442, 1127.
Nataf, D.M. et al., 2010, ApJ 721, L28
Nordström, B., et al. 2004, A&A, 418, 989
Ruchti, G. R., et al. 2010, ApJ721, L92
Rybka, S.P., 2008, KPCB 24, 99
Siebert, A., Bienaymé, O., & Soubiran, C. 2003, A&A399, 531
Siebert, A., et al. 2008, MNRAS, 391 793
Soubiran, C., Bienayme, O., Siebert, A., 2003, A&A 399, 531
Soubiran, C., & Girard, P., 2005, A&A 438, 139.
Soubiran, C., Bienayme, O., Mishenina, T.V., Kovtyukh, V.V., 2008, A&A 480, 91
Steinmetz, M., et al. 2006, AJ132, 1645
Takeda, Y., Sato, B., & Murata, D., 2008, PASJ 60, 781.
Valentini, U. & Munari, U., 2010, A&A 522, A79
Veltz, L., et al. 2008, A&A480, 753
Zwitter, T., & Munari, U., 2000, An introduction to analysis of single dispersion spectra with IRAF, Asiago monographs vol. 1, Osservatori Astronomici di Padova e Asiago Pub.
Zwitter, T., et al. 2008, AJ136, 421
Zwitter, T., et al. 2010, A&A 522, A54